RADIO SCIENCE, VOL. 43, RS1012, doi:10.1029/2007RS003696, 2008

Properties of the transformation from the spherical wave expansion to the plane wave expansion

Cecilia Cappellin,[1,2] Olav Breinbjerg,[1] and Aksel Frandsen[2]

Received 16 May 2007; revised 2 October 2007; accepted 12 November 2007; published 12 February 2008.

[1] The transformation between the spherical wave expansion (SWE) and the plane wave expansion (PWE) is investigated with respect to a range of its fundamental properties. First, the transformation of individual spherical waves is studied in order to understand how these contribute to the different regions of the plane wave spectrum. Second, the number of spherical waves necessary to accurately determine the PWE over different regions of the spectral domain is investigated. Third, numerical aspects of the transformation are addressed.

Citation: Cappellin, C., O. Breinbjerg, and A. Frandsen (2008), Properties of the transformation from the spherical wave expansion to the plane wave expansion, *Radio Sci.*, *43*, RS1012, doi:10.1029/2007RS003696.

1. Introduction

[2] The spherical wave expansion (SWE) and the plane wave expansion (PWE) are two well-known techniques to express time-harmonic electromagnetic fields in source-free regions of space. While the SWE expresses the field as an infinite series of discrete spherical waves, the PWE expresses the field as an infinite continuous spectrum of plane waves. Each of these expansions exists in slightly different forms, e.g., with different expansion functions and different spectral domains, but these forms are all equivalent. The original form of the SWE was introduced by *Hansen* [1935], while the theory was popularized a few years later by *Stratton* [1941]. A more recent treatment was given by *Hansen* [1988] in relation to spherical near-field antenna measurements. The original PWE was introduced by *Whittaker and Watson* [1927], reformulated by *Stratton* [1941], employed by *Kerns* [1976] for planar near-field antenna measurements, and recently treated by *Hansen and Yaghjian* [1999]. One form of the PWE employs as spectral variables the Cartesian components of the wave propagation vector [*Hansen and Yaghjian*, 1999], while another form employs instead its spherical components [*Stratton*, 1941]. The SWE and PWE have been extensively employed in both the optical and microwave frequency bands in areas like propagation and diffraction theory, imaging techniques, and antenna measurements [*Devaney*, 1982; *Hansen and Johansen*, 2000; *Mehler*, 1988; *Yaghjian*, 1986]. The choice of employing the SWE or the PWE is determined by the geometry of the source configuration, the spatial region of interest, and the available information about the radiated fields.

[3] Though the SWE and the PWE can both be derived from the homogeneous vector Helmholtz equation, their regions of validity are fundamentally different. Employing a Cartesian (x, y, z)-coordinate system and the associated spherical (r, θ, φ)-coordinate system, the SWE is valid for all $r > r_o$, where r_o is the largest r-coordinate of the source and hence the radius of the so-called *minimum sphere*, while the PWE is valid for all $z > z_o$ where z_o is the largest z-coordinate of the source, see Figure 1. It is noted, for later use, that r_o is obviously always larger than or equal to z_o, i.e., $r_o \geq |z_o|$. For source regions with a planar aperture, the PWE will, by a proper orientation of the coordinate system, be valid in the extreme near-field of the aperture while this will not be the case for the SWE, see Figure 1.

[4] While the mathematical formulations of the PWE and SWE are very different, as are their respective regions of validity, it can be shown that it is possible to derive one expansion from the other through a rigorous transformation. The necessary equations to perform the transformation, i.e. the PWE of the spherical vector wave functions of the SWE, were first presented by *Stratton* [1941, p. 417] and later by *Morse and Feshbach* [1953, p. 1865]. A complete treatment of the transformation was given by *Devaney and Wolf* [1974] and recently by *Varadan et al.* [1991]. These works on the SWE-to-PWE transformation concentrate on its mathematical derivation, while such aspects as convergence mechanism and truncation of the series and integrals involved in the transformation, as well as its

[1] Ørsted•DTU, Technical University of Denmark, Lyngby, Denmark.
[2] TICRA, Copenhagen, Denmark.

0048-6604/08/2007RS003696$11.00

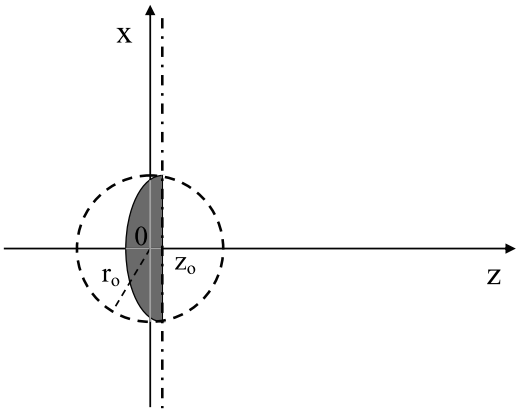

Figure 1. Spatial domains of validity of the SWE and PWE for a general antenna: the PWE is valid for $z > z_o$, the SWE for $r > r_o$.

numerical implementation, have been dealt with to a lesser degree.

[5] It is thus the primary purpose of the present work to investigate the fundamental properties of the SWE-to-PWE transformation. The transformation of individual spherical waves will be studied in order to understand how these contribute to the different regions of the plane wave spectrum. Also, the number of spherical waves necessary to accurately determine the PWE over different regions of the plane wave spectrum will be investigated. Furthermore, numerical aspects of the transformation will be addressed.

[6] The SWE-to-PWE transformation is particularly useful in antenna diagnostics for spherical near-field antenna measurements [*Cappellin et al.*, 2006a, 2006b]. Electrical and mechanical errors in an antenna may seriously affect the antenna performance, and while their presence is normally detected by anomalies in the measured far-field pattern, often only an analysis of the extreme near-field can allow their identification. However, the computation of the extreme near-field is generally not possible when the field is expressed as a SWE obtained from a spherical near-field measurement, since the SWE is valid only outside the antenna minimum sphere of radius r_o. One way to overcome this limitation is to transform the SWE into the PWE, which is valid on any z-plane $z > z_o$, with $|z_o| \leq r_o$. Once the PWE is known, the extreme near-field can be computed and subjected to the diagnostics. For this use, it is particularly interesting to note that the SWE-to-PWE transformation provides the contributions of the spherical waves in the visible as well as invisible regions of the spectral domain. The contribution of the invisible region of the PWE to the extreme near-field can be significant at distances less than one wavelength from the antenna [*Yaghjian*, 1986; *Wang*, 1988], and it gives a spatial resolution better than the half wavelength provided by the visible region of the PWE [*Booker and Clemmow*, 1950].

[7] The present manuscript focuses on fundamental properties of the SWE-to-PWE transformation that constitutes an essential step in this antenna diagnostics technique but does not document the diagnostics technique as such. The fundamental properties of the SWE-to-PWE transformation do have practical implications for the antenna diagnostics technique but this relies also on other essential steps [see, e.g., *Cappellin et al.*, 2006a, 2006b], and it is documented in more practically oriented works [*Cappellin et al.*, 2007a, 2007b].

[8] The present manuscript is organized as follows: In section 2 the SWE and PWE are briefly summarized with attention to their definitions and regions of validity. In section 3 the derivation of the SWE-to-PWE transformation is described and its fundamental properties are discussed in detail. In section 4 a test case is presented for numerical investigation. All expressions are given in the S.I. rationalized system with a suppressed $e^{-i\omega t}$ time convention.

2. Spherical Wave Expansion and Plane Wave Expansion

[9] We begin by introducing the SWE of the electric field $\overline{E}$ radiated by an antenna enclosed in a minimum sphere of radius r_o [*Hansen*, 1988],

$$\overline{E}(\overline{r}) = \frac{k}{\sqrt{\eta}} \sum_{n=1}^{\infty} \sum_{m=-n}^{n} Q_{1mn}^{(3)} \overline{F}_{1mn}^{(3)}(\overline{r}) + Q_{2mn}^{(3)} \overline{F}_{2mn}^{(3)}(\overline{r}), \quad r > r_o \tag{1}$$

with η being the medium intrinsic admittance, k the wave number, and $\overline{r}$ the position vector expressed in spherical coordinates (r, θ, φ). The expansion coefficients are denoted by $Q_{1mn}^{(3)}$ and $Q_{2mn}^{(3)}$, while $\overline{F}_{1mn}^{(3)}(\overline{r})$ and $\overline{F}_{2mn}^{(3)}(\overline{r})$ are the power-normalized spherical vector wave functions given by

$$\overline{F}_{1mn}^{(3)}(\overline{r}) = \frac{1}{\sqrt{2\pi}} \frac{1}{\sqrt{n(n+1)}} \left(-\frac{m}{|m|}\right)^m \cdot \left\{ h_n^{(1)}(kr) \frac{im}{\sin\theta} \overline{P}_n^{|m|}(\cos\theta) e^{im\varphi} \hat{\theta} - h_n^{(1)}(kr) \frac{d}{d\theta} \overline{P}_n^{|m|}(\cos\theta) e^{im\varphi} \hat{\varphi} \right\} \tag{2}$$

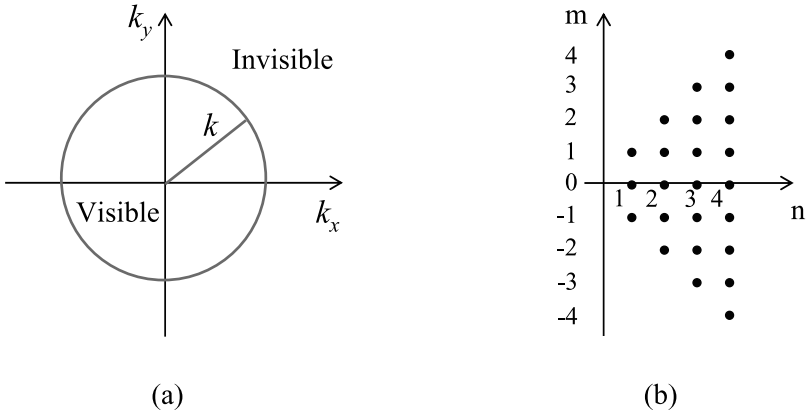

Figure 2. (a) Visible and invisible regions of the spectral $k_x k_y$-domain of the PWE, (b) *nm*-modes in the SWE.

$$\overline{F}^{(3)}_{2mn}(\bar{r}) = \frac{1}{\sqrt{2\pi}} \frac{1}{\sqrt{n(n+1)}} \left(-\frac{m}{|m|}\right)^m \cdot \left\{ \frac{n(n+1)}{kr} h_n^{(1)}(kr) \overline{P}_n^{|m|}(\cos\theta) e^{im\varphi} \hat{r} + \frac{1}{kr} \frac{d}{d(kr)} \left(kr h_n^{(1)}(kr)\right) \frac{d}{d\theta} \overline{P}_n^{|m|}(\cos\theta) e^{im\varphi} \hat{\theta} + \frac{1}{kr} \frac{d}{d(kr)} \left(kr h_n^{(1)}(kr)\right) \frac{im}{\sin\theta} \overline{P}_n^{|m|}(\cos\theta) e^{im\varphi} \hat{\varphi} \right\} \tag{3}$$

In these expressions $h_n^{(1)}(kr)$ is the spherical Hankel function of the first kind, $\overline{P}_n^{|m|}(\cos\theta)$ the normalized associated Legendre function of degree n and order m [*Hansen*, 1988, equation (A1.25)], and $\hat{r}, \hat{\theta}, \hat{\varphi}$ are the spherical unit vectors. It can be seen from equations (2) and (3) that the r-dependence of the spherical vector wave functions is given by $h_n^{(1)}(kr)$. For each spherical mode with index n a transition region exists around $r_n = n/k$, since the mode decays rapidly with increasing r for $r \ll r_n$, corresponding to an evanescent wave, while it decays as r^{-1} for $r \gg r_n$, corresponding to a propagating wave. Though all modes are thus propagating in the far-field, this transition property implies that, for an antenna with a minimum sphere radius r_o, the high-order modes with $n > kr_o$ are highly suppressed outside the minimum sphere and only modes with $n < kr_o$ contribute to the far-field. Hence, the n-series in equation (1) can be truncated at $N \cong kr_o + 10$ while maintaining a high accuracy of the far-field [*Hansen*, 1988].

[10] The PWE of the same electric field $\overline{E}$ in the spectral $k_x k_y$-domain valid for $z > z_o$, with z_o being the largest z-coordinate of the antenna, is given by [*Hansen and Yaghjian*, 1999]

$$\overline{E}(\bar{r}) = \frac{1}{2\pi} \int_{-\infty}^{\infty} \int_{-\infty}^{\infty} \overline{T}(k_x, k_y) e^{ik_z z} e^{i\left(k_x x + k_y y\right)} dk_x dk_y, \quad z > z_o \tag{4}$$

where $\bar{r}$ is the position vector with Cartesian coordinates (x, y, z) and k_x, k_y are the spectral variables, which, together with $k_z = \sqrt{k^2 - k_x^2 - k_y^2}$, constitute the Cartesian components of the wave propagation vector $\bar{k}$, $\bar{k} = k_x\hat{x} + k_y\hat{y} + k_z\hat{z}$. $\overline{T}(k_x, k_y)$ is the plane wave spectrum at $z = 0$, while $\overline{T}(k_x, k_y)e^{ik_z z}$ is the spectrum for a given z-coordinate. The spectral domain is divided in two regions, the visible region for $k_x^2 + k_y^2 \le k^2$, and the invisible region for $k_x^2 + k_y^2 > k^2$, see Figure 2a. While the spectral variables k_x and k_y are real everywhere, k_z is real in the visible region and purely imaginary with a positive imaginary part in the invisible region. Real values of k_z correspond to propagating plane waves, while imaginary values of k_z correspond to evanescent plane waves that are exponentially attenuated with z. Their contribution is usually negligible at distances larger than one wavelength from the antenna [*Yaghjian*, 1986; *Wang*, 1988]. In practice, the k_x- and k_y-integrals in equation (4) are truncated at finite values $\pm k_{x\max}$ and $\pm k_{y\max}$, respectively. At the border between the visible and invisible regions $k_z = 0$ and a singularity of the type $1/k_z$ is generally present in at least one component of the plane wave spectrum $\overline{T}$ [*Hansen and Yaghjian*, 1999]. A necessary

but not sufficient condition to avoid such a singularity is that the antenna far-field pattern exhibits a null for $\theta = \pi/2$. It is finally recalled that a simple relation exists between the far-field and the visible region of the plane wave spectrum, according to [*Hansen and Yaghjian*, 1999, equation (3.133); *Booker and Clemmow*, 1950],

$$\overline{E}_{far}(r,\theta,\varphi) = \lim_{kr\to\infty} \overline{E}(r,\theta,\varphi) = -\frac{e^{ikr}}{r} ik\cos\theta\, \overline{T}(k\sin\theta\cos\varphi, k\sin\theta\sin\varphi)$$
$$\theta \in [0,\pi/2], \quad \varphi \in [0,2\pi] \tag{5}$$

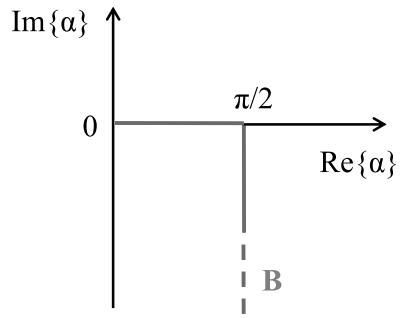

Figure 3. Domain of the variable α on contour B.

3. SWE-to-PWE Transformation and Its Properties

3.1. Theory

[11] It will now be shown how the SWE of equation (1) can be transformed into the PWE of equation (4). The following derivation is based on *Devaney and Wolf* [1974]; however, it has been extended [*Cappellin et al.*, 2006b] in order to use the power-normalized spherical vector wave functions, the $k_x k_y$-PWE, and the S.I. system of units. The use of the power-normalized spherical vector wave functions turns out to be particular advantageous since these are employed in the textbook [*Hansen*, 1988] and in the software SNIFTD (homepage of SNIFTD, http://www.ticra.dk/script/site/page.asp?artid=27), which have become widely used standards for spherical near-field antenna measurements. There are alternative derivations of the SWE-to-PWE transformation, and one such approach is given in Appendix A. The transformation will be derived in three steps.

[12] The first step consists of introducing the PWE of the spherical vector wave functions, and since *Devaney and Wolf* [1974] employs the spectral $\alpha\beta$-domain we thus take outset in

$$\overline{F}^{(3)}_{1mn}(\overline{r}) = \frac{(-i)^{n+1}}{2\pi\sqrt{n(n+1)}} \int_{-\pi}^{\pi} \int_{B} \overline{Y}^m_n(\alpha,\beta)\, e^{ik\hat{k}\cdot\overline{r}} \cdot \sin\alpha\, d\alpha\, d\beta \tag{6}$$

$$\overline{F}^{(3)}_{2mn}(\overline{r}) = \frac{(-i)^{n}}{2\pi\sqrt{n(n+1)}} \int_{-\pi}^{\pi} \int_{B} \hat{k}\times\overline{Y}^m_n(\alpha,\beta)\, e^{ik\hat{k}\cdot\overline{r}} \cdot \sin\alpha\, d\alpha\, d\beta \tag{7}$$

with $\hat{k} = \overline{k}/k = \sin\alpha\cos\beta\,\hat{x} + \sin\alpha\sin\beta\,\hat{y} + \cos\alpha\,\hat{z}$ being the unit wave propagation vector, the spectral variable β belonging to the interval $[-\pi, \pi]$ and the spectral variable α belonging to the complex contour B, see Figure 3. Real values of α correspond to propagating waves, while complex values of α correspond to evanescent waves. The function $\overline{Y}^m_n(\alpha, \beta)$ is the vector spherical harmonics which can be expressed as

$$\overline{Y}^m_n(\alpha,\beta) = -\frac{i}{\sqrt{2\pi}}\left(-\frac{m}{|m|}\right)^m \left(\frac{d}{d\alpha}\overline{P}^{|m|}_n(\cos\alpha)e^{im\beta}\hat{\beta} - \frac{im}{\sin\alpha}\overline{P}^{|m|}_n(\cos\alpha)e^{im\beta}\hat{\alpha}\right) \tag{8}$$

with $\hat{\alpha} = \cos\alpha\cos\beta\,\hat{x} + \cos\alpha\sin\beta\,\hat{y} - \sin\alpha\,\hat{z}$ and $\hat{\beta} = -\sin\beta\,\hat{x} + \cos\beta\,\hat{y}$.

[13] Second, the PWEs of equations (6) and (7) are substituted into the SWE of equation (1), and the order of integration and summation is interchanged, obtaining the PWE of the electric field in the spectral $\alpha\beta$-domain

$$\overline{E}(\overline{r}) = \frac{k}{2\pi}\int_{-\pi}^{\pi}\int_{B} \tilde{E}(\hat{k})\, e^{ik\hat{k}\cdot\overline{r}} \sin\alpha\, d\alpha\, d\beta \tag{9}$$

where the spectrum complex amplitude $\tilde{E}(\hat{k})$ is given by

$$\tilde{E}(\hat{k}) = \sum_{n=1}^{\infty}\sum_{m=-n}^{n} \frac{(-i)^n}{\sqrt{\eta}\sqrt{n(n+1)}} \cdot \left[-iQ^{(3)}_{1mn}\overline{Y}^m_n(\alpha,\beta) + Q^{(3)}_{2mn}\hat{k}\times\overline{Y}^m_n(\alpha,\beta)\right]. \tag{10}$$

Thus, the spectrum complex amplitude can be calculated from the knowledge of the SWE coefficients $Q^{(3)}_{1mn}$ and $Q^{(3)}_{2mn}$.

[14] Third, the spectrum in the spectral $\alpha\beta$-domain, $\tilde{E}(\hat{k})e^{ik\cos\alpha\, z}$, is translated into the $k_x k_y$-domain obtaining $\overline{T}(k_x, k_y)e^{ik_z z}$, since it can be shown that

$$\overline{T}(k_x,k_y)\, e^{ik_z z} = \frac{1}{k_z}\tilde{E}(\hat{k})\, e^{ik\cos\alpha\, z} \tag{11}$$

where α and β on the right hand side are expressed as functions of the spectral variables k_x and k_y according to

$$\alpha = \arcsin\left(\sqrt{\frac{k_x^2 + k_y^2}{k^2}}\right) \text{ and } \beta = \arctan\left(\frac{k_y}{k_x}\right) \quad (12)$$

Obviously the arcsin and arctan functions must be implemented to ensure the correct contour B for the angle α and the interval $[-\pi, \pi]$ for the angle β.

[15] Equation (11) is derived by applying to equation (9) a change in the integration variables using $k_x = k \sin\alpha \cos\beta$, $k_y = k \sin\alpha \sin\beta$, $k_z = k \cos\alpha$, and by identifying the obtained result with equation (4). With equation (12), the α- and β-values corresponding to chosen k_x- and k_y-values can be calculated exactly without interpolation. By combining equations (10)–(12), the plane wave spectrum $\overline{T}(k_x, k_y)e^{ik_z z} = \overline{T}(k_x, k_y, z)$ can finally be written as

$$\overline{T}(k_x, k_y, z) = \sum_{n=1}^{\infty} \sum_{m=-n}^{n} Q_{1mn}^{(3)} \overline{T}_{1mn}(k_x, k_y, z) + Q_{2mn}^{(3)} \overline{T}_{2mn}(k_x, k_y, z) \quad (13)$$

where

$$\overline{T}_{1mn}(k_x, k_y, z) = \frac{e^{ik_z z}}{k_z} \frac{(-i)^{n+1}}{\sqrt{\eta}\sqrt{n(n+1)}} \overline{Y}_n^m(\alpha, \beta) \quad (14)$$

$$\overline{T}_{2mn}(k_x, k_y, z) = \frac{e^{ik_z z}}{k_z} \frac{(-i)^{n}}{\sqrt{\eta}\sqrt{n(n+1)}} \hat{k} \times \overline{Y}_n^m(\alpha, \beta) \quad (15)$$

[16] In order to calculate the PWE of equation (4) from the known SWE of equation (1) we can summarize the required steps as follows:

[17] 1. Choose a certain $k_x k_y$-spectral domain according to the desired spatial resolution (see later).

[18] 2. For every point in the $k_x k_y$-spectral domain, determine the corresponding α- and β-values from equation (12).

[19] 3. Calculate the plane wave spectrum at the chosen z-plane with equation (13).

[20] It is emphasized that equations (6), (7), and (10) are of fundamental importance in the theory of modal expansions and provide the theoretical justification for the SWE-to-PWE transformation. In particular it is noted that the spectrum complex amplitude $\tilde{E}(\hat{k})$ is an analytic function in its complex domain of definition, since it can be expressed by the spatial Fourier transform of the finite source distributions [*Devaney and Wolf*, 1974; *Gerchberg*, 1974]. Second, $\tilde{E}(\hat{k})$ is a vector function normal to the unit vector $\hat{k}$, i.e., $\hat{k} \cdot \tilde{E}(\hat{k}) = 0$. Third, the vector spherical harmonics $\overline{Y}_n^m(\alpha, \beta)$ and $\hat{k} \times \overline{Y}_n^m(\alpha, \beta)$ constitute a complete orthogonal basis for all analytical vector functions normal to the unit vector $\hat{k}$ [*Devaney and Wolf*, 1974]. Thus equation (10) becomes the necessary intermediate step for the transformation from the SWE to the PWE, or vice-versa. It is finally noted that though we begin with a SWE that is only valid outside the minimum sphere, $r > r_o$, the obtained PWE is valid also inside the minimum sphere for all points with $z > z_o$ since $\tilde{E}(\hat{k})$ is independent of z.

3.2. Fundamental Properties

[21] We will now discuss some fundamental properties of the SWE-to-PWE transformation related to resolution, exponential growth of the spherical vector wave functions, and transformation of individual spherical modes.

[22] First, once the plane wave spectrum $\overline{T}(k_x, k_y, z)$ is computed through equation (13), the spatial resolution along the x- and y-directions, δ_x and δ_y, of the electric field obtained from equation (4) is given by $\delta_x = \pi/k_{x\,\max}$, $\delta_y = \pi/k_{y\,\max}$. A spatial resolution better than half a wavelength, $\lambda/2$, is thus provided when part of the invisible region is taken into account, since either k_x, k_y or both are larger than the wavenumber $k = 2\pi/\lambda$. Here, the resolution is defined as the spatial distance between the nulls of the fastest oscillating spectral component. On the other hand, for a given desired spatial resolution, δ_x and δ_y, the required range of the PWE is obtained from $k_{x\,\max} = \pi/\delta_x$ and $k_{y\,\max} = \pi/\delta_y$, and this range will then determine the number of modes in the SWE and thus the truncation number N (see later).

[23] Second, from equations (2), (3), and (8) we observe that

$$\overline{Y}_n^m(\alpha, \beta) \propto \overline{K}_{1mn}(\alpha, \beta)$$
$$\hat{k} \times \overline{Y}_n^m(\alpha, \beta) \propto \overline{K}_{2mn}(\alpha, \beta) \quad (16)$$

where $\overline{K}_{smn}(\theta, \varphi) = \lim_{kr\to\infty} \frac{kr}{e^{ikr}} \overline{F}_{smn}^{(3)}(r, \theta, \varphi)$, with $s = 1, 2$, is the far-field pattern function of the spherical vector waves [*Hansen*, 1988]. Thus, the computation of $\tilde{E}(\hat{k})$ by equation (10) corresponds to the SWE of the far-field. This implies that all information about the visible and invisible spectral regions of the plane wave spectrum is in principle contained in the far-field. However, while the traditional truncation in the n-index at $N = kr_o + 10$ provides accurate values of the SWE of the electric far-field [*Hansen*, 1988] and thus of the spectrum $\overline{T}(k_x, k_y)$ in the visible region, the same truncation value will in general not be sufficient in the invisible region as it will be shown below. The reason for different convergence rates in the two regions lies in the fact that the invisible region is described by complex values of the spectral variable α, see Figure 3. The trigonometric functions in α appearing in the associated Legendre functions

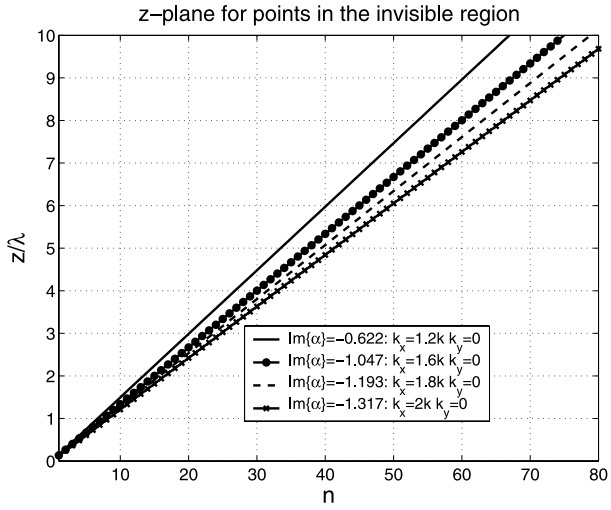

Figure 4. Relation between the z-plane and the degree n for different points of the invisible region, according to equation (18).

contained in $\overline{Y}_n^m(\alpha, \beta)$, see equations (8), (14), and (15), are not limited in the complex domain described by the contour B. This has two consequences: The first one is that computational problems appear in the evaluation of the associated Legendre functions in the invisible region already for moderate values of n. The second one is that the exponential growth of these functions requires Q coefficients of extremely low values, normally provided by high n- and m-modes, in order for the series of equation (13) to reach convergence. While the exponential growth of the trigonometric functions in the invisible region is an inherent mathematical property, we notice however that the transformation of equations (13)–(15) does not require the calculation of the vector spherical harmonics $\overline{Y}_n^m(\alpha, \beta)$ themselves but rather their product with the function $\exp(ik_z z)$, which is exponentially decaying in the invisible region. The exponential growth of the vector spherical harmonics can thus be limited by embedding the term $\exp(ik_z z)$ into the computation of $\overline{Y}_n^m(\alpha, \beta)$ for complex values of α and choosing the z-plane appropriately. The intermediate computation of the extremely large values contained in the vector spherical harmonics is thus avoided since the product with $\exp(ik_z z)$ is automatically considered. This procedure also reduces the computation time of equation (13). If the associated Legendre functions are computed through the rotation coefficients defined by *Hansen* [1988, equations (A2.17-18-19)], it is found that the embedding of the factor $\exp(ik_z z)$ results in a sum of exponential terms where the largest contribution is $f(n, \alpha, z)$ given by

$$f(n, \alpha, z) = \exp(-n\mathrm{Im}\{\alpha\} + k\, z \sinh(\mathrm{Im}\{\alpha\})) \quad (17)$$

with α belonging to the domain B depicted in Figure 3, and n being the degree of the associated Legendre function $\overline{P}_n^{|m|}(\cos\alpha)$ in equation (8). Hence, for a given point in the invisible region of the plane wave spectrum characterized by a negative value of $\mathrm{Im}\{\alpha\}$, and a given term in the SWE characterized by the index n, equation (17) shows that the exponent can be kept bounded and less than a certain value S provided that the z-coordinate is chosen according to

$$z > \frac{S + n\mathrm{Im}\{\alpha\}}{k \sinh(\mathrm{Im}\{\alpha\})} \quad (18)$$

Equation (18) can thus be used as a guideline to select the appropriate z-plane for a given point in the invisible region and the maximum $n = N$ in the series of equation (13). In Figure 4 the relation of equation (18) is illustrated for different values of n, z and $\mathrm{Im}\{\alpha\}$ in the case of $S = 0$. For example, if $\mathrm{Im}\{\alpha\} = -1.317$, corresponding to $k_x = 2k$ (crossed line), and if $n = 50$, the z-plane should be selected larger than 6λ. It is noted that the z-plane given by equation (18) is normally too large for the purpose of diagnostics where only the extreme near-field is of interest. However, since the z-dependence of the plane wave spectrum $\overline{T}$ is given by $\exp(ik_z z)$, we are allowed to choose with equation (18) a certain z-plane to make the computation of the single terms of equation (13) more efficient, and then back-propagate the result of the double summation of equation (13) to a new z_2-plane, $z_2 < z$, which is the one of interest for the diagnostics. This can be accomplished by simply multiplying by $\exp(-ik_z \Delta z)$, with $\Delta z = z - z_2$.

[24] In order to provide an insight into how the plane wave spectrum depends on the n- and m- spherical modes and to better understand how a given spherical wave transforms and contributes to the visible and invisible regions of the spectral $k_x k_y$-domain, we now concentrate on equations (14) and (15) and study the behavior of $\overline{T}_{1mn}$ and $\overline{T}_{2mn}$ on the z-plane $z = 0$ with varying n and m. We first note that the magnitudes $|\overline{T}_{1mn}| = |\overline{T}_{1-mn}| = |\overline{T}_{2mn}| = |\overline{T}_{2-mn}|$ and that these are azimuthally constant since the β dependence is given by $e^{im\beta}$. We can then choose either a fixed n-mode and vary the m-modes, $|m| = 0, 1, \ldots, n$, or a fixed m-mode and vary the n-modes, $n = \max(1, |m|), \ldots, N$, see Figure 2b. For a fixed n-mode, see Figure 5 for the case of $n = 3$, we observe that every m-mode with $|m| \neq 1$ provides a null at $k_x = k_y = 0$, and this null is surrounded by a circular region of low magnitude with a radius that increases for increasing m, in accordance with the well-know property that only modes with $|m| = 1$ are nonzero on the z-axis. We also notice that the smaller the $|m|$, the larger the value of $|\overline{T}_{1mn}|$ in the invisible region, again see Figure 5. For a fixed m-mode, see Figure 6 for the case $m = 0$, there is an annular null inside the visible region, with a

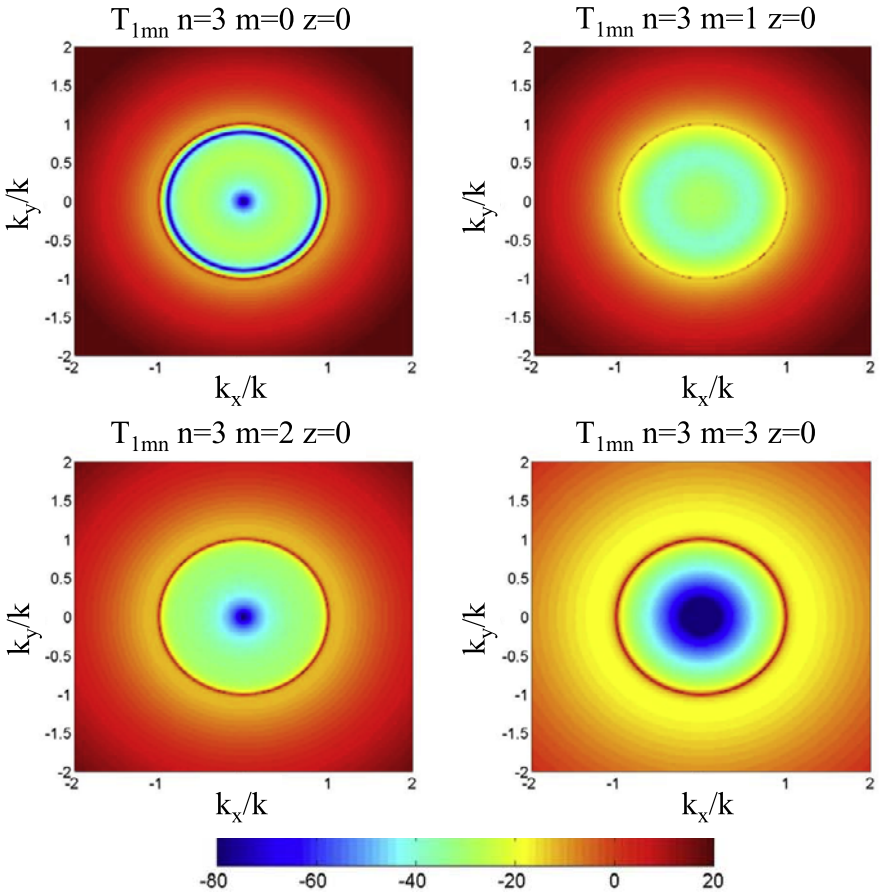

Figure 5. Magnitude $|\overline{T}_{1mn}|$ in dB for $n = 3$ and $m = 0, 1, 2, 3$ on the plane $z = 0$.

radius that decreases for increasing n. We finally observe that for larger n, the period of oscillation of $|\overline{T}_{1mn}|$ inside the visible region becomes smaller, and the magnitude in the invisible region becomes larger, again see Figure 6.

[25] All these observations are useful in understanding the mapping of a given spherical wave into the spectral $k_x k_y$-domain. It should be kept in mind however that what happens in the general case of a series of spherical waves is more complicated, since the spherical waves are weighted by the coefficients $Q^{(3)}_{1mn}$ and $Q^{(3)}_{2mn}$. The influence of the expansion coefficients on equation (13) will be analyzed through an extensive numerical investigation in section 4, where the possibility of truncating the infinite n-modes to a finite N will be also taken into account.

[26] It is finally noticed that the number of terms contained in equation (13) for a given truncation in the n-modes equal to N, is given by $2N\cdot(N+2)$. If the extents of the spectral $k_x k_y$-domain are given by $2k_{x\max}$ and $2k_{y\max}$ along the k_x- and k_y-axis, respectively, then, for chosen sampling densities δk_x and δk_y, $R = (2k_{x\max}/\delta k_x) + 1$ points will be present in k_x and $V = (2k_{y\max}/\delta k_y) + 1$ points in k_y. Thus, the total number of terms that must be calculated in equation (13) is $R \cdot V \cdot 2N \cdot (N + 2)$, where each term is of the form of equation (14) or (15).

3.3. A Simple Test Case: Electric Hertzian Dipole at the Origin

[27] In order to illustrate the SWE-to-PWE transformation and the computation of the visible as well as invisible regions of the plane wave spectrum from the Q coefficients of the SWE, we consider a z-oriented electric Hertzian dipole with dipole moment p located at the origin of the coordinate system.

[28] For this antenna configuration we know from *Hansen* [1988, equation (2.117)] that the SWE of the radiated field contains only the single mode $s = 2$, $m = 0$, $n = 1$, where

$$Q^{(3)}_{201} = -\frac{kp}{\sqrt{\eta 6\pi}} \tag{19}$$

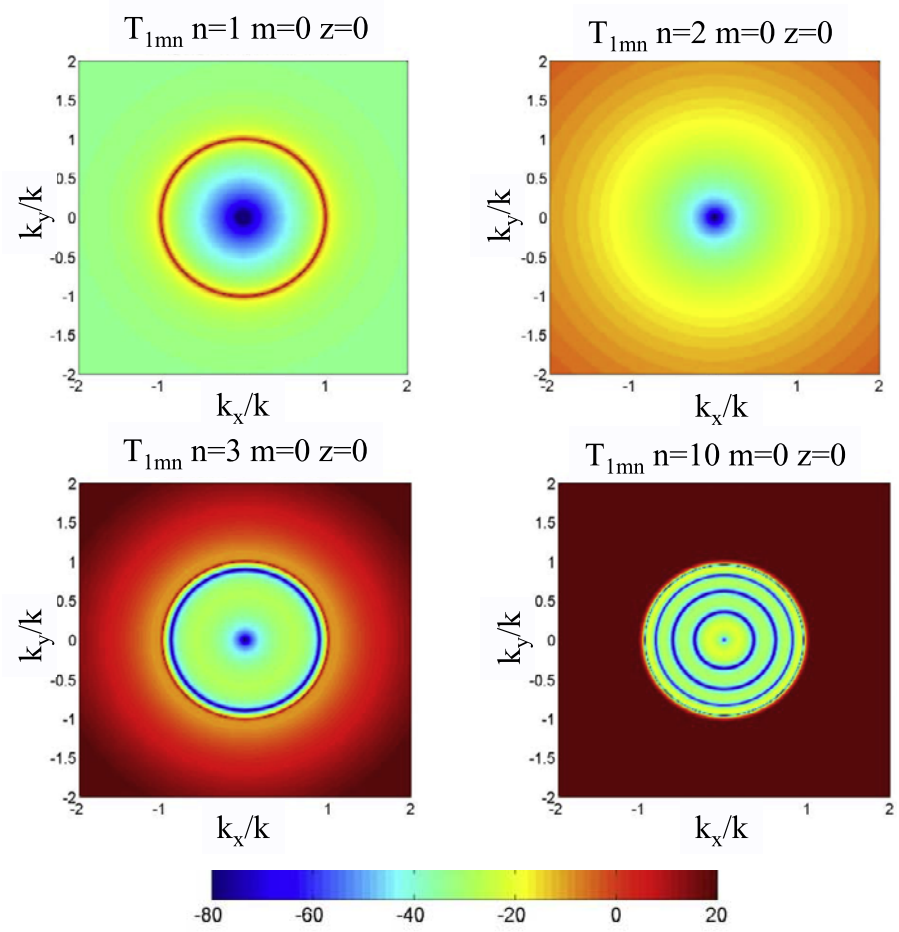

Figure 6. Magnitude $|\overline{T}_{1mn}|$ in dB for $m = 0$ and $n = 1, 2, 3, 10$ on the plane $z = 0$.

$$\overline{F}^{(3)}_{201}(\bar{r}) = \frac{\sqrt{6}}{2\sqrt{\pi}}\left(\frac{h_1^{(1)}(kr)}{kr}\cos\theta\,\hat{r} - \frac{1}{2}\frac{1}{kr}\frac{d}{d(kr)}\left(krh_1^{(1)}(kr)\right)\sin\theta\,\hat{\theta}\right) \quad (20)$$

When equation (19) is substituted into equation (13) and equation (12) is used, the plane wave spectrum becomes

$$\overline{T}(k_x, k_y, z) = \frac{p}{4\pi k\eta}\left(k_x\hat{x} + k_y\hat{y} + \frac{k_z^2 - k^2}{k_z}\hat{z}\right)e^{ik_z z}, \quad (21)$$

which agrees with the plane wave spectrum obtained directly from the dipole current [*Hansen and Yaghjian*, 1999, equation (3.109)]. Though this configuration is particularly simple, it illustrates the general property that each spherical vector wave contributes to the entire spectral domain of the PWE – the visible region as well as the invisible region – and that the complete PWE can be obtained from the complete SWE. For a general antenna more Q coefficients will be present in the SWE of the radiated field, and thus more terms will be required in the computation of equation (13) as illustrated in the following section.

4. Numerical Investigation on the SWE-to-PWE Transformation

[29] In this section we investigate the properties of the SWE-to-PWE transformation of equation (13), in particular the convergence mechanism, in the general case where the coefficients $Q^{(3)}_{1mn}$ and $Q^{(3)}_{2mn}$ are included. The purpose is to study the possibility of truncating the infinite n-series to a finite value N that might be different from the truncation number used in far-field calculations. In order to do that, we investigate the case of an x-oriented electric Hertzian dipole displaced on the x-axis, see Figure 7. In spite of its apparent simplicity, this test

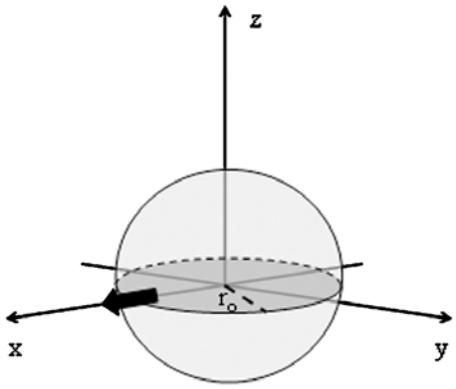

Figure 7. *x*-oriented electric Hertzian dipole displaced along the *x*-axis at a distance r_o from the origin.

case possesses characteristics that are representative for more complex antennas, and its use here is motivated by several factors. First, since any source distribution can in principle be constructed from a combination of properly positioned, oriented and excited Hertzian dipoles, the case of a single dipole is representative for more realistic sources. Second, as it will be seen in equations (22) and (23), a single electric Hertzian dipole displaced from the origin of the coordinate system possesses an infinite SWE like any complex antenna, which allows us to study the truncation of equation (13) to finite *N*-values. Third, the Hertzian dipole allows the analytical calculation of the exact plane wave spectrum which provides the necessary reference to investigate such a truncation, see equations (24)–(26). We have investigated other source configurations, see, for example, *Cappellin et al.* [2006a, 2006b] for an array of Hertzian dipoles and a rectangular aperture in free-space, but the present one with a single dipole shows qualitatively – though not quantitatively – the same properties.

[30] For the *x*-oriented dipole with dipole moment *p* located at the position $x = r_o$ the *Q* coefficients can be calculated analytically [*Hansen*, 1988, equation (A1.78)]

$$Q^{(3)}_{1mn} = 0 \qquad n = 1, 2, ..\infty \quad m = -n, .., n \tag{22}$$

$$Q^{(3)}_{2mn} = \frac{-kp}{\sqrt{\eta}} \left(-\frac{m}{|m|} \right)^m \frac{\sqrt{n(n+1)}}{\sqrt{2\pi}} \frac{j_n(kr_o)}{kr_o} \overline{P}^{|m|}_n(0)$$
$$n = 1, 2, ..\infty \quad m = -n, .., n \tag{23}$$

with $j_n(kr)$ being the spherical Bessel function of the first kind. Different values of r_o have been studied and here the results for $r_o = 2\lambda$, corresponding to $kr_o = 12$, are presented. The *n*-mode power spectrum, $P_{rad}(n) = \frac{1}{2}\sum_{s=1}^{2}\sum_{m=-n}^{n}\left|Q^{(3)}_{smn}\right|^2$ [*Hansen*, 1988, equation (2.55)], normalized to the value of P_{rad} (1), is shown in Figure 8. It is seen that the peak occurs at $n \approx kr_o = 12$, as expected, and that the major amount of power is contained in the first $N = kr_o + 10$ modes. By use of equations (12), (13), (22), and (23) the plane wave spectrum is calculated for different truncation numbers *N* and resolved in its Cartesian components T_x, T_y, and T_z. These are then compared to the exact plane wave spectrum, calculated analytically from the dipole current distribution as [*Hansen and Yaghjian*, 1999, equation (3.109)]

$$T_{ref\ x} = \frac{p}{4\pi k\eta} \frac{k_x^2 - k^2}{k_z} e^{-ik_x r_o} e^{ik_z z} \tag{24}$$

$$T_{ref\ y} = \frac{p}{4\pi k\eta} \frac{k_x k_y}{k_z} e^{-ik_x r_o} e^{ik_z z} \tag{25}$$

$$T_{ref\ z} = \frac{p}{4\pi k\eta} k_x e^{-ik_x r_o} e^{ik_z z} \tag{26}$$

From equations (24)–(26) it is seen that $T_{ref\ x}$ and $T_{ref\ y}$ contain the singularity in k_z. Figure 9 shows the normalized magnitude (in logarithmic scale) of the *x*-component, $T_{ref\,x}$ and T_x, on the plane $z = 0.2\lambda$, for $N = kr_o$, $N = kr_o + 10$, $N = kr_o + 20$, $N = kr_o + 30$, and $N = kr_o + 38$, while the corresponding phase plots in radians are given in Figure 10. From Figure 9 it is possible to distinguish the singularity for $k_z = 0$, the nulls occurring at $k_x = \pm k$, and the exponential decay in the invisible region. Equation (13) is a convergent series, and we notice from

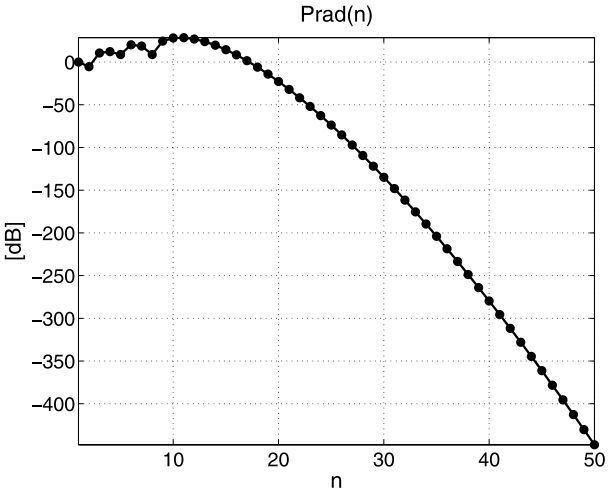

Figure 8. *n*-mode power spectrum for the *x*-oriented Hertzian dipole, with $r_o = 2\lambda$.

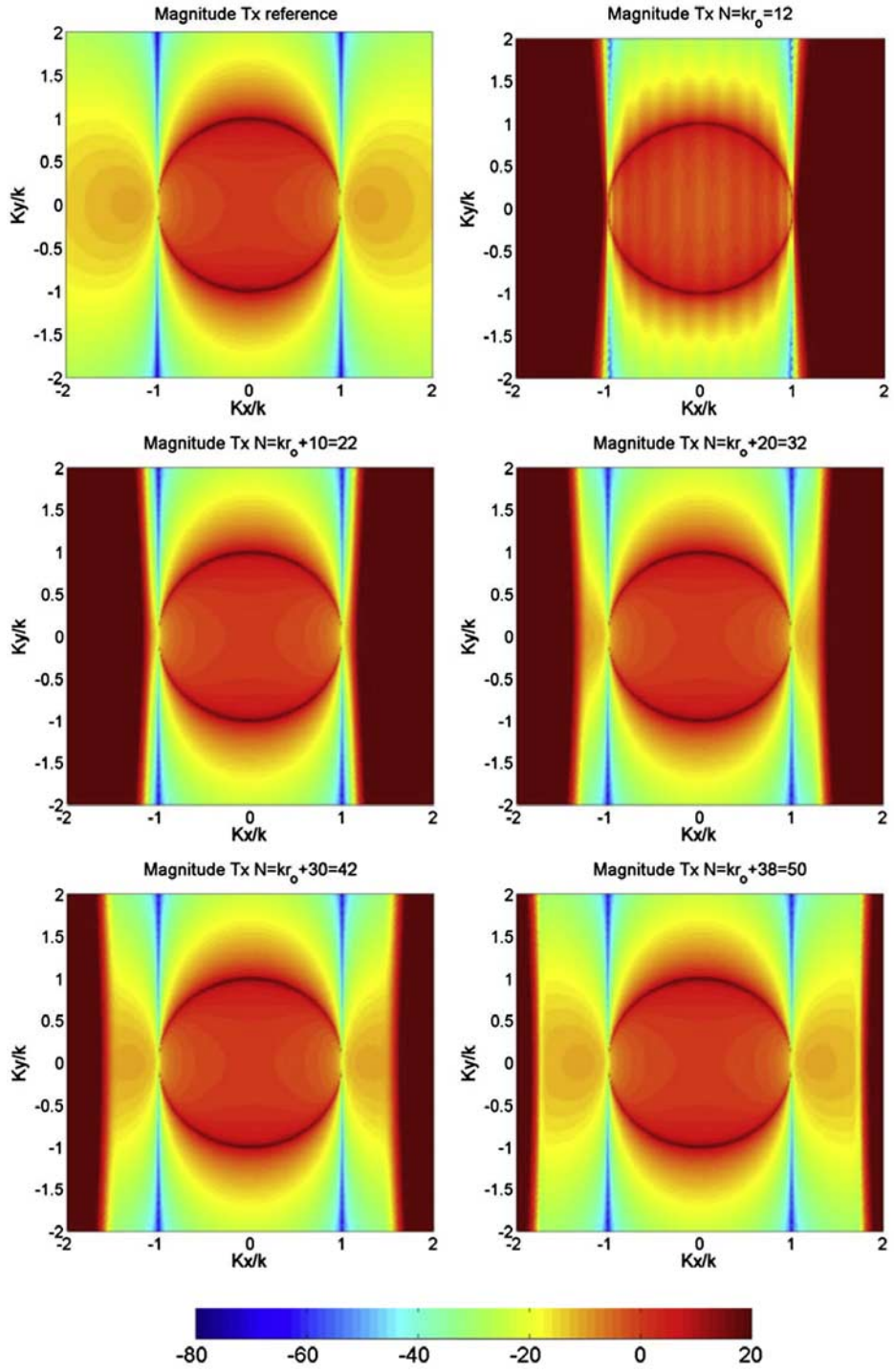

Figure 9. Magnitude of T_x in dB for $r_o = 2\lambda$ on $z = 0.2\lambda$: the reference $T_{ref\,x}$ and T_x for $N = kr_o$, $N = kr_o + 10$, $N = kr_o + 20$, $N = kr_o + 30$ and $N = kr_o + 38$.

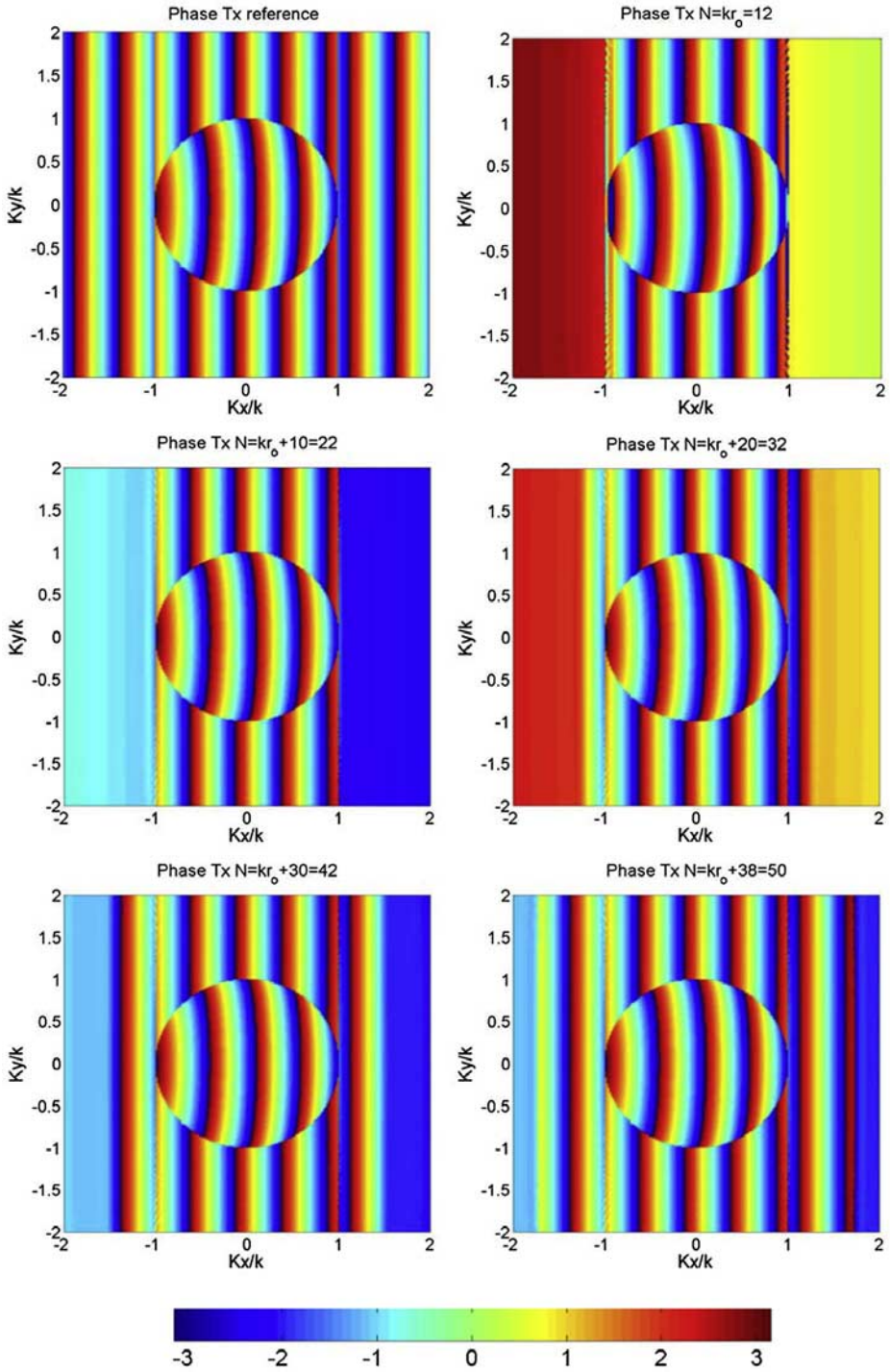

Figure 10. Phase of T_x in radians for $r_o = 2\lambda$ on $z = 0.2\lambda$: the reference $T_{ref\,x}$ and T_x for $N = kr_o$, $N = kr_o + 10$, $N = kr_o + 20$, $N = kr_o + 30$ and $N = kr_o + 38$.

Figure 9 that the spectral region in the $k_x k_y$-domain where the convergence is reached gradually increases with increasing N. For $N = kr_o = 12$ the visible region is not completely reconstructed but the convergence is reached with $N = kr_o + 10 = 22$, in the visible region and at $k_z = 0$. Values of $N > kr_o + 10$ only influence the invisible region.

[31] The convergence mechanism can also be understood by considering the n-mode power spectrum of Figure 8. The extremely low values of power contained in the high n-modes are given by corresponding extremely low values of Q-coefficients which keep finite the product with the diverging spherical vector wave functions, and provide the necessary terms in order for the series of equation (13) to reach convergence. A plot of the amplitude of T_x as a function of N for specific points in the spectral domain is shown in Figure 11. We clearly distinguish two different mechanisms: the series of equation (13) reaches convergence with $N = kr_o + 10 = 22$ for points in the visible region, while additional N terms are needed to reach convergence for points in the invisible region. In particular, for the spectral point (k_x, k_y) = (1.2k, 0) (solid line in Figure 11 below), convergence is not reached until $N = \mathrm{kr}_o + 23 = 35$. For the spectral point (k_x, k_y) = (1.6k, 0) (line with circles in Figure 11 below) convergence is not reached until $N = \mathrm{kr}_o + 33 = 45$; and for ($k_x$, k_y) = (1.8k, 1.8k) (line with squares in Figure 11 below) convergence is not within the first 50 terms of the SWE. Furthermore, it is interesting to note that for these spectral points the magnitude of the accumulated series becomes very large, in excess of 100 dB, for intermediate values of N before it converges at a level of some −10 dB. For all of these spectral points in the invisible region, the first few terms ($N < 5$) are bounded and the accumulated series has values comparable to those for points in the visible region. A plot of the real and imaginary parts of T_x as a function of N, see Figure 12, shows that the path to convergence for points with $k_y = 0$ and $k_x > k$ forms a rectangular spiral which initially diverges but then converges to the final value. For points within the visible region, the convergence path is more irregular though obviously much faster. It has been observed that these mechanisms of convergence are independent of the spectral component and govern both the amplitude and the phase. The truncation number N required to reach convergence in the [−2k, 2k] domain depends on r_o and it has been found that $N = kr_o + 4kr_\mathrm{o}$ constitutes a good rule-of-thumb. This rule holds for the present case of a single dipole and was also observed for other antenna configurations [*Cappellin et al.*, 2006a, 2006b], though it may not be generally valid. Moreover, as a consequence of the properties of the expansion of equation (10), the

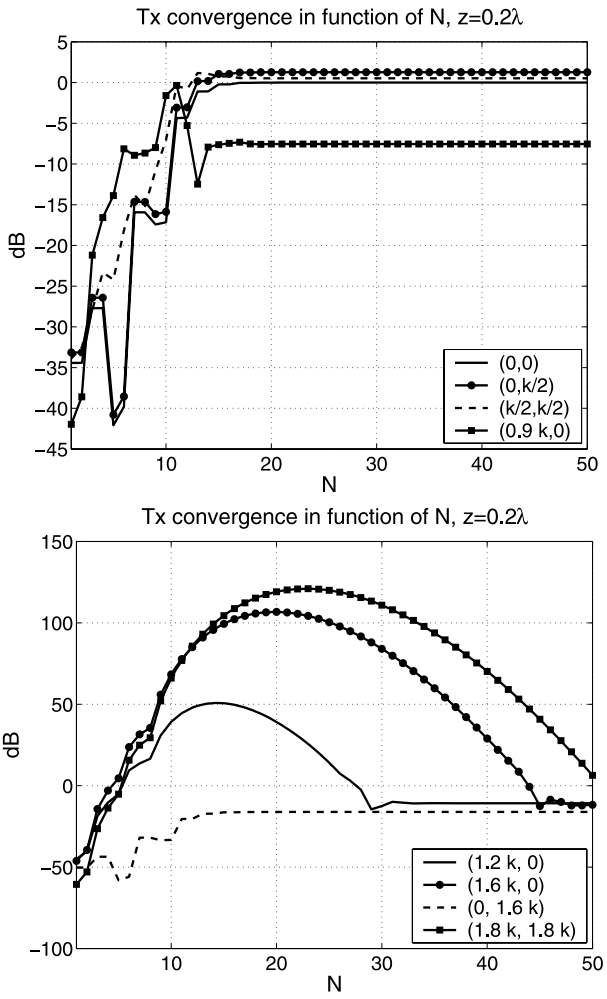

Figure 11. Magnitude of T_x in dB for $r_o = 2\lambda$ on $z = 0.2\lambda$ as a function of N, for different points of the spectral domain.

convergence mechanism is independent of the z-plane of observation though the spectrum in the invisible region of course becomes negligible with larger z-coordinates, see Figure 13 for the case $z = 4\lambda$. Since the Hertzian dipole investigated here is displaced along the x-axis, the convergence of the SWE-to-PWE transformation depends only on the k_x spectral variable and is thus independent of the k_y spectral variable as seen from Figures 9–10. For sources distributed along both the x- and y-axes, the convergence will depend on both k_x and k_y in the sense that all points in the visible region reach convergence with $N = kr_o + 10$, while all points in the

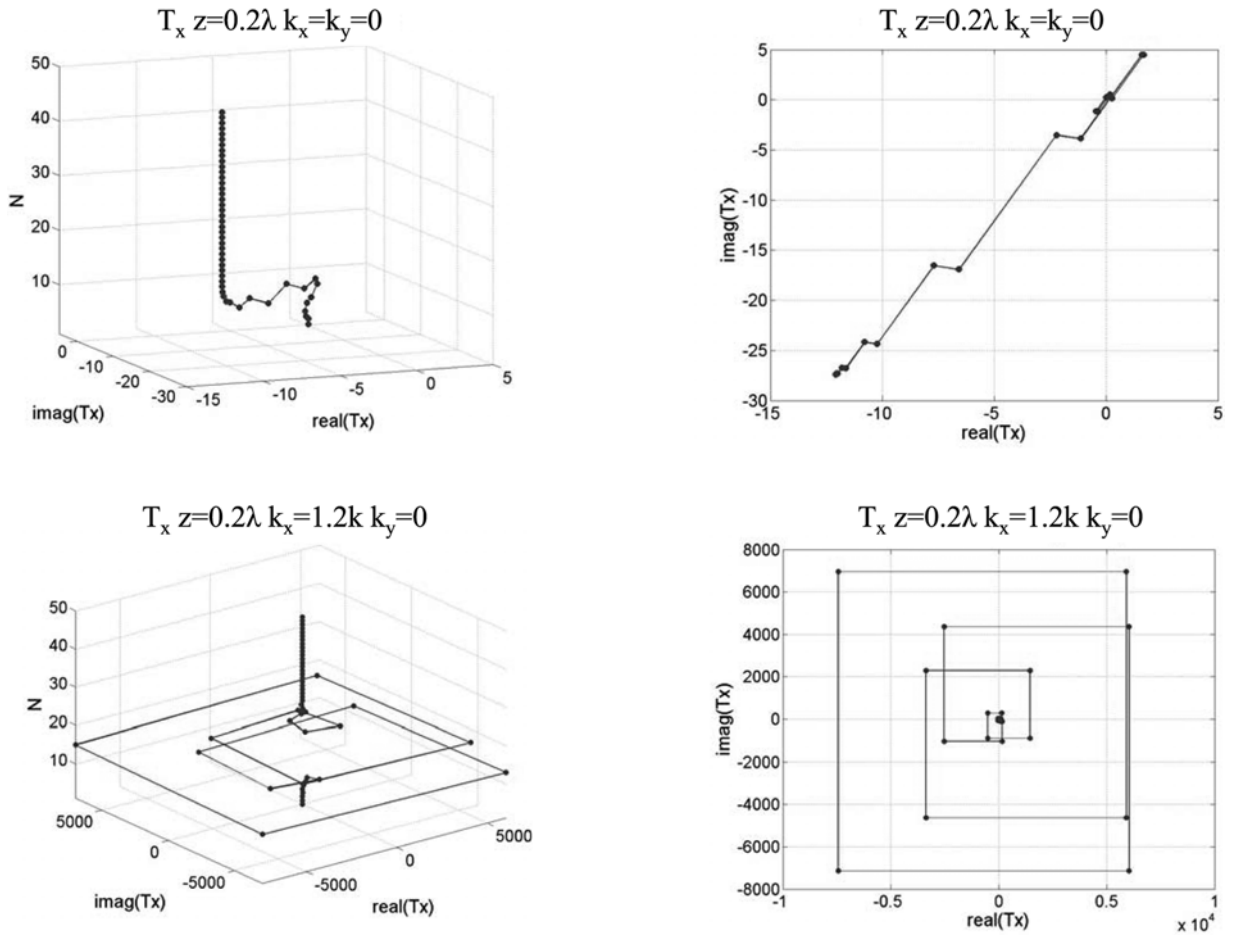

Figure 12. Real and imaginary parts of T_x in linear scale for $r_o = 2\lambda$ on $z = 0.2\lambda$ as a function of N: 3-D and 2-D plots of a point in the visible and one in the invisible region.

invisible require more terms depending on their location in the spectral domain and the antenna size.

5. Conclusions

[32] Fundamental properties of the SWE-to-PWE transformation have been investigated analytically and numerically. The transformation allows the calculation of the PWE in the visible as well as the invisible spectral regions from the knowledge of the Q-coefficients of the SWE. The transformation of individual spherical waves was studied in order to determine how these contribute to different regions of the spectral domain. It was noted that each spherical wave contributes to the visible as well as the invisible regions and thus provides information on the propagating as well as evanescent waves of the PWE. Also, the convergence properties of the transformation were studied, and it was found that these are vastly different for the visible and invisible regions of the PWE. While a truncation in the n-modes at $N = kr_o + 10$, with r_o being the radius of the minimum sphere, is generally sufficient to reach convergence in the visible region, a much higher value is necessary in the invisible region, where the path to convergence was found to involve very large intermediate values. For the configuration investigated here, a truncation number $N = kr_o + 4\ kr_o$ was found to be necessary for a $[-2k, 2k]$ region of the spectral domain. Furthermore, it was shown how the numerical problem of calculating the spherical wave functions for a given n- and m-mode in points of the invisible region can be overcome by embedding the $\exp(ik_z z)$ term in the calculation of the associated Legen-

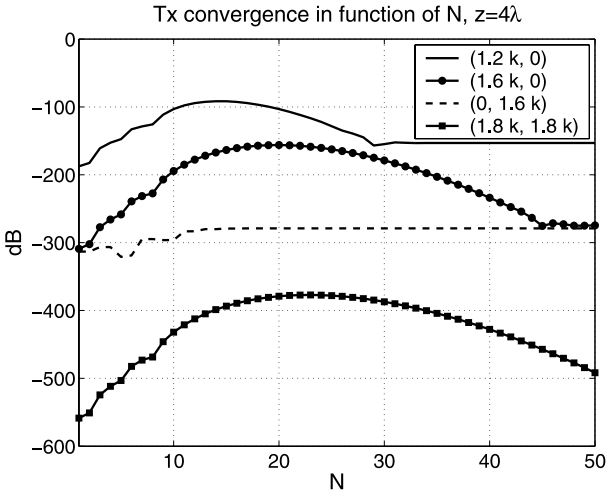

Figure 13. Magnitude of T_x in dB for $r_o = 2\lambda$ on $z = 4\lambda$ as a function of N, for points of the invisible region.

dre functions, and guidelines were provided to find the proper z-plane. Finally, it was pointed out that the determination of the PWE in the invisible region leads to an improved spatial resolution compared to the traditional half a wavelength provided by the visible region alone.

[33] The SWE-to-PWE transformation constitutes an essential step in a new antenna diagnostics technique for spherical near-field antenna measurements, where the extreme near-field must subsequently be computed from the obtained PWE using equation (4) by either a direct numerical integration or, more efficiently, an inverse Fourier transform [*Cappellin et al.*, 2006b]. It is noted that the antenna diagnostics technique based on the SWE-to-PWE transformation will be influenced and limited by the finite dynamic range and accuracy of the measurement system. This will limit the number of terms in the SWE that can be accurately measured and the spectral region where convergence can be reached [*Cappellin et al.*, 2006a, 2007a, 2007b]. Nevertheless, the properties of the SWE-to-PWE transformation investigated above are generally also of practical importance and determine, along with the quality of the measurement system, the accuracy and the efficiency of this antenna diagnostics technique [*Cappellin et al.*, 2007a, 2007b].

Appendix A

[34] In this appendix the SWE-to-PWE transformation is derived along the lines of *Hansen and Yaghjian* [1999, section 3]. We begin by introducing the far-field expression for the SWE of equation (1) [*Hansen*, 1988, equation (2.179)],

$$\begin{aligned}\overline{E}_{far}(\overline{r}) &= \lim_{kr\to\infty} \overline{E}(\overline{r}) \\ &= \frac{e^{ikr}}{r}\frac{1}{\sqrt{\eta}}\frac{1}{\sqrt{4\pi}}\sum_{n=1}^{\infty}\sum_{m=-n}^{n} Q^{(3)}_{1mn}\overline{K}_{1mn}(\theta,\varphi) \\ &\quad + Q^{(3)}_{2mn}\overline{K}_{2mn}(\theta,\varphi) \\ &= \frac{e^{ikr}}{r}\overline{F}(\theta,\varphi) \end{aligned} \tag{A1}$$

with $\theta \in [0, \pi]$ and $\varphi \in [0, 2\pi]$. $\overline{F}(\theta, \varphi)$ is the far-field pattern, and $\overline{K}_{smn}(\theta, \varphi)$ the far-field pattern functions [*Hansen*, 1988, p. 49]

$$\overline{K}_{smn}(\theta,\varphi) = \lim_{kr\to\infty} \frac{\sqrt{4\pi}kr}{e^{ikr}}\overline{F}^{(3)}_{smn}(r,\theta,\varphi) \qquad s = 1, 2 \tag{A2}$$

$$\overline{K}_{1mn}(\theta,\varphi) = \sqrt{\frac{2}{n(n+1)}}\left(-\frac{m}{|m|}\right)^m e^{im\varphi}(-i)^{n+1} \cdot \left[\frac{im\overline{P}^{|m|}_n(\cos\theta)}{\sin\theta}\hat{\theta} - \frac{d\overline{P}^{|m|}_n(\cos\theta)}{d\theta}\hat{\varphi}\right] \tag{A3}$$

$$\overline{K}_{2mn}(\theta,\varphi) = \sqrt{\frac{2}{n(n+1)}}\left(-\frac{m}{|m|}\right)^m e^{im\varphi}(-i)^{n} \cdot \left[\frac{d\overline{P}^{|m|}_n(\cos\theta)}{d\theta}\hat{\theta} + \frac{im\overline{P}^{|m|}_n(\cos\theta)}{\sin\theta}\hat{\varphi}\right] \tag{A4}$$

Next, we consider the PWE of equation (4) and in particular its far-field expression in equation (5) [*Hansen and Yaghjian*, 1999, equation (3.133)]

$$\begin{aligned}\overline{E}_{far}(\overline{r}) &= \lim_{kr\to\infty} \overline{E}(\overline{r}) \\ &= -\frac{e^{ikr}}{r} ik\cos\theta\, \overline{T}(k\sin\theta\cos\varphi, k\sin\theta\sin\varphi) \\ &= \frac{e^{ikr}}{r}\overline{F}(\theta,\varphi) \end{aligned} \tag{A5}$$

with $\theta \in [0, \pi/2], \varphi \in [0, 2\pi]$. By identifying equations (A1) and (A5) in the spatial domain where both hold, $\theta \in$

$[0, \pi/2]$ $\varphi \in [0, 2\pi]$, the plane wave spectrum $\overline{T}$ can be expressed as

$$\overline{T}(k\sin\theta\cos\varphi, k\sin\theta\sin\varphi) = \frac{i}{\sqrt{\eta}}\frac{1}{\sqrt{4\pi}}\frac{1}{k\cos\theta}\sum_{n=1}^{\infty}\sum_{m=-n}^{n} Q_{1mn}^{(3)}\overline{K}_{1mn}(\theta,\varphi) + Q_{2mn}^{(3)}\overline{K}_{2mn}(\theta,\varphi) = \frac{i}{k\cos\theta}\overline{F}(\theta,\varphi) \tag{A6}$$

where $k\sin\theta\cos\varphi = k_x$ and $k\sin\theta\sin\varphi = k_y$ are the spectral variables. In the first place, this relation holds for real θ-angles and thus the visible region, $k_x^2 + k_y^2 \le k^2$. However, since the far-field pattern of a finite source distribution is an analytic function [*Hansen and Yaghjian*, 1999; *Gerchberg*, 1974], it is possible to analytically continue the far-field pattern to complex θ-angles, obtaining from equations (A6) the plane wave spectrum also in the invisible region, $k_x^2 + k_y^2 > k^2$. While the relationship between the plane wave spectrum and the far-field pattern can be found from equation (A5) alone, the use of equation (A1), and thus of the first equality in equation (A6), allows the analytical continuation to complex values of θ, overcoming the difficulty of continuing a measured far-field pattern [*Hansen and Yaghjian*, 1999, p. 136].

[35] By writing θ and φ as functions of the spectral variables k_x and k_y according to

$$\theta = \arcsin\left(\sqrt{\frac{k_x^2 + k_y^2}{k^2}}\right), \quad \varphi = \arctan\left(\frac{k_y}{k_x}\right) \tag{A7}$$

allowing values of k_x and k_y larger than k and ensuring $\theta \in B$ and $\varphi \in [0, 2\pi]$, writing $k_z = k\cos\theta$ and by defining $\overline{T}(k_x, k_y)e^{ik_z z} = \overline{T}(k_x, k_y, z)$, from equation (A6) it follows that

$$\overline{T}(k_x, k_y, z) = \sum_{n=1}^{\infty}\sum_{m=-n}^{n} Q_{1mn}^{(3)}\overline{T}_{1mn}(k_x, k_y, z) + Q_{2mn}^{(3)}\overline{T}_{2mn}(k_x, k_y, z) \tag{A8}$$

where

$$\overline{T}_{1mn}(k_x, k_y, z) = \frac{e^{ik_z z}}{k_z}\frac{i}{\sqrt{4\pi}\sqrt{\eta}}\overline{K}_{1mn}(\theta,\varphi) \tag{A9}$$

$$\overline{T}_{2mn}(k_x, k_y, z) = \frac{e^{ik_z z}}{k_z}\frac{i}{\sqrt{4\pi}\sqrt{\eta}}\overline{K}_{2mn}(\theta,\varphi) \tag{A10}$$

The plane wave spectrum $\overline{T}(k_x, k_y, z)$ can thus be written in its entire $k_x k_y$-domain from the knowledge of the Q coefficients of the SWE of the radiated field.

References

Booker, H. G., and P. C. Clemmow (1950), The concept of an angular spectrum of plane waves, and its relations to that of polar diagram and aperture distribution, *Proc. Inst. Elec. Eng.*, *97*, 11–17.

Cappellin, C., O. Breinbjerg, and A. Frandsen (2006a), The influence of finite measurement accuracy on the SWE-to-PWE antenna diagnostics technique, paper presented at EuCAP European Conference on Antennas and Propagation, Nice, France.

Cappellin, C., A. Frandsen, and O. Breinbjerg (2006b), On the relationship between the spherical wave expansion and the plane wave expansion for antenna diagnostics, paper presented at AMTA Europe Symposium, Munich, Germany.

Cappellin, C., A. Frandsen, and O. Breinbjerg (2007a), Application of the SWE-to-PWE antenna diagnostics technique to an offset reflector antenna, paper presented at AMTA Antenna Measurements Technique Association Symposium, St. Louis, Mo.

Cappellin, C., A. Frandsen, S. Pivnenko, G. Lemanczyk, and O. Breinbjerg (2007b), Diagnostics of the SMOS radiometer antenna system at the DTU-ESA spherical near-field antenna test facility, paper presented at EuCAP European Conference on Antennas and Propagation, Edinburgh, UK.

Devaney, A. J. (1982), A filtered backpropagation algorithm for diffraction tomography, *Ultrason. Imag.*, *4*, 336–360.

Devaney, A. J., and E. Wolf (1974), Multipole expansion and plane wave representations of the electromagnetic field, *J. Math. Phys.*, *15*, 234–244.

Gerchberg, R. W. (1974), Super-resolution through error energy reduction, *Opt. Acta*, *21*, 709–720.

Hansen, J. E. (Ed.) (1988), *Spherical Near-Field Antenna Measurements*, Peter Peregrinus, London.

Hansen, T. B., and P. M. Johansen (2000), Inversion scheme for ground penetrating radar that takes into account the planar air-soil interface, *IEEE Trans. Geosci. Remote Sens.*, *38*, 496–506.

Hansen, T. B., and A. D. Yaghjian (Eds.) (1999), *Plane Wave Theory of Time-Domain Fields, Near-Field Scanning Applications*, IEEE Press, New York.

Hansen, W. W. (1935), A new type of expansion in radiation problems, *Phys. Rev.*, *47*, 139–143.

Kerns, D. M. (1976), Plane wave scattering-matrix theory of antennas and antenna-antenna interactions: Formulation and applications, *J. Res. Natl. Bur. Stand., Sect. B*, *80*, 5–51.

Mehler, M. J. (1988), Application of spherical wave expansions to direct GO far field synthesis, *Microwaves Antennas Propag., IEE Proc., Part H*, *135*, 41–47.

Morse, P., and H. Feshbach (Eds.) (1953), *Methods of Theoretical Physics*, *Int. Ser. Pure Appl. Phys.*, McGraw-Hill, New York.

Stratton, J. A. (Ed.) (1941), *Electromagnetic Theory*, McGraw-Hill, New York.

Varadan, V. V., A. Lakhtakia, and V. K. Varadan (Eds.) (1991), *Field Representations and Introduction to Scattering*, Elsevier, Amsterdam.

Wang, J. J. H. (1988), An examination of the theory and practices of planar near/field measurement, *IEEE Trans. Antennas Propag.*, *36*, 746–753.

Whittaker, G. T., and G. N. Watson (Eds.) (1927), *Modern Analysis*, Cambridge Univ. Press, London.

Yaghjian, A. D. (1986), An overview of near-field antenna measurements, *IEEE Trans. Antennas Propag.*, *34*, 30–45.

O. Breinbjerg, Ørsted•DTU, Technical University of Denmark, DK-2800 Kgs. Lyngby, Denmark. (ob@oersted.dtu.dk)

C. Cappellin and A. Frandsen, TICRA, Læderstræde 34, DK-1201 Copenhagen K, Denmark. (cc@ticra.com; af@ticra.com)